Journal of Molecular Spectroscopy 408 (2025) 111986

Contents lists available at ScienceDirect

Journal of Molecular Spectroscopy

journal homepage: www.elsevier.com/locate/yjmsp

Rotational spectrum of trifluoroacetic acid: Extension of the measurements by chirped-pulse spectroscopy

Greta Naso [a], Filippo Baroncelli [a,*], Luca Evangelisti [b,c,d], Assimo Maris [a,b], Sonia Melandri [a,b,c]

[a] Department of Chemistry G. Ciamician, University of Bologna, Bologna, I-40126, Italy
[b] Interdepartmental Centre for Industrial Aerospace Research (CIRI Aerospace), University of Bologna, Cesena, I-47521, Italy
[c] Interdepartmental Centre for Industrial Agrifood Research (CIRI Agrifood), University of Bologna, Forlì, I-47121, Italy
[d] Department of Chemistry G. Ciamician, Campus of Ravenna, University of Bologna, Ravenna, I-48123, Italy

ARTICLE INFO

Dataset link: https://doi.org/10.6092/unibo/amsacta/8016

Keywords:
Rotational spectroscopy
Chirped-pulse Fourier transform microwave spectroscopy
Perfluoroalkyl carboxylic acid
Organic acids

ABSTRACT

The rotational spectrum of trifluoroacetic acid has been recorded at room temperature in the 18–26 GHz frequency range using a chirped-pulse Fourier transform microwave (CP-FTMW) spectrometer. More than 180 new spectral lines have been identified and assigned to transitions within the vibrational ground state. A global fitting has been performed by incorporating spectroscopic data from previous studies, leading to the refinement of the molecular parameters. Two fitting models using Watson's *S*-reduction and *A*-reduction are proposed, allowing the determination of h_3 for the first model and Φ_{JK}, Φ_{KJ}, and ϕ_K for the second one.

1. Introduction

Trifluoroacetic acid (TFA, CF_3COOH) is the smallest perfluoroalkyl carboxylic acid (PFCA), composed of a fluorocarbon tail (CF_3) and a carboxylic (COOH) terminal group. TFA is considered a volatile organic compound (VOC), but also fully miscible in water and classified as very persistent and very mobile (vPvM). TFA is released into the environment by various anthropogenic sources [1] whereas its natural occurrence is still debated [2]. TFA is produced synthetically for use in the chemical industry and it is also formed as a by-product of the degradation of some hydrochlorofluorocarbons (HCFC) and hydrofluorocarbons (HFC) used mainly as refrigerants as well as hydrofluoroolefins (HFO) [3]. However, its concentrations in certain environmental compartments have considerably increased over the last decades [2] being now order of magnitudes higher than those of other per- and polyfluoroalkyl substances (PFAS) [1]. Microwave spectroscopy is a suitable technique for monitoring this class of compounds in the atmosphere [4–6]. A variety of PFCA has already been studied with this techniques, starting from TFA [7–9] to other linear molecules with progressively longer carbon chains, such as: perfluoropropionic acid (CF_3CF_2COOH [10]), perfluorobutyric acid ($CF_3(CF_2)_2COOH$ [11]), perfluoropentanoic acid ($CF_3(CF_2)_3COOH$ [12]) and perfluorooctanoic acid (PFOA, $CF_3(CF_2)_6COOH$ [13]). For all systems only the global minimum conformer has been observed and assigned except for perfluorooctanoic acid for which six conformers were observed and assigned. For all of them, only the *cis* conformation of the hydroxyl group with respect to the carbonyl unit has been observed.

Focusing on TFA, multiple studies of the molecule's rotational spectrum have been performed over the years. In 1985 Stolwijk and van Eijck published the first microwave spectroscopy study on TFA, performed in the range 17 to 40 GHz using a conventional cell [7]. The recorded spectrum was complicated and additional measurements employing radiofrequency-microwave double resonance (rf-mw DR) and microwave–microwave double resonance (mw–mw DR) techniques were used for the identification of the observed features. These methods allowed for the assignment of rotational transitions of the vibrational ground state and the vibrational excited states of the C–C torsion mode, up to $v = 4$. A hyperfine structure of the spectrum due to the -CF_3 internal rotation tunnelling effect was observed for $v = 3$, 4 and 5, and the internal rotation barrier was determined $V_3 = 241.8(5)$ cm^{-1}. Further measurements on the deuterated form TFA-D allowed the determination of the position of the hydroxyl hydrogen atom, confirming that its orientation is *cis* to the C=O group. No other conformers were observed.

In 1999 Antolinez et al. published the spectra of TFA and TFA-D recorded in the 1–24 GHz frequency region using two different

* Corresponding author.
E-mail addresses: greta.naso@studio.unibo.it (G. Naso), filippo.baroncelli2@unibo.it (F. Baroncelli), luca.evangelisti6@unibo.it (L. Evangelisti), assimo.maris@unibo.it (A. Maris), sonia.melandri@unibo.it (S. Melandri).

https://doi.org/10.1016/j.jms.2025.111986
Received 22 November 2024; Received in revised form 2 January 2025; Accepted 8 January 2025
Available online 22 January 2025

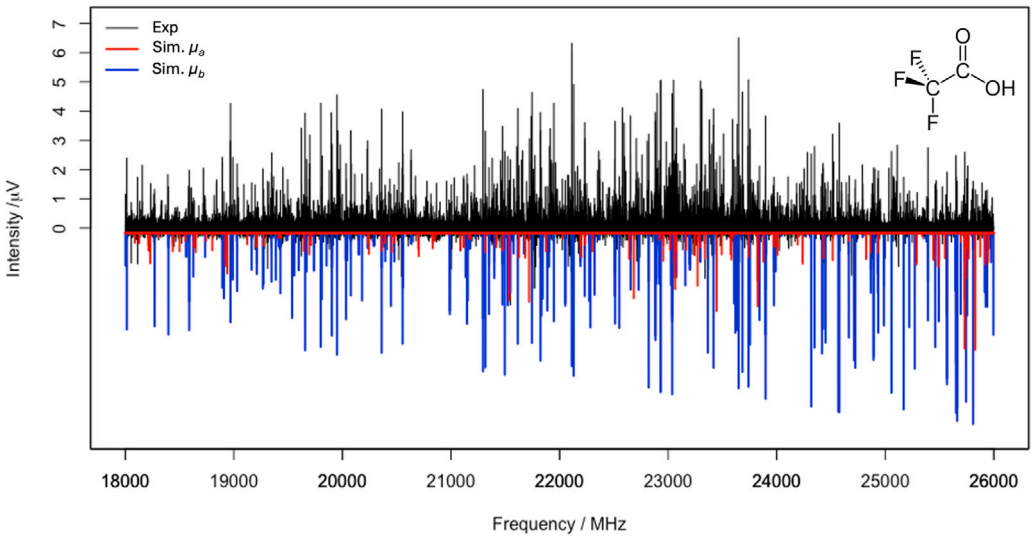

Fig. 1. Room temperature CP-FTMW spectrum of TFA recorded with 400,000 signal averages (black upper trace) with the simulation of μ_a-type (red lower trace) and μ_b-type (blue lower trace) spectrum at T = 303 K.

molecular beam Fourier transform microwave (MB-FTMW) spectrometers [8]. New transitions were reported and the deuterium nuclear quadrupole coupling constants were determined. Moreover, the ^{13}C and ^{18}O isotopologues were observed in natural abundance allowing for the determination of a partial substitution structure.

In 2007, during the MB-FTMW investigation of the hydrated clusters of TFA in the 6.5–18 GHz spectral region, Ouyang et al. measured some new transition lines of the TFA monomer [9]. As regards the observed TFA:water$_{1,2,3}$ species, all adopt a closed-ring structure stabilized by hydrogen bonds. Based on these results it was estimated that 8% of TFA is expected to form the monohydrated species under typical atmospheric conditions.

Many advancements have been made, particularly in developing chirped-pulse Fourier transform microwave (CP-FTMW) spectroscopy, which has revolutionized the field since its invention in 2006 [14]. This technique allows for the collection of broadband, high-resolution microwave spectra at a rate several orders of magnitude faster than traditional methods. As a result, it has significantly enhanced the determination of molecular structures, particularly for increasingly complex systems. The ability to rapidly acquire spectral data has opened up new possibilities in molecular spectroscopy, enabling the study of larger molecules and reactive intermediates, as well as facilitating more detailed investigations into chemical kinetics and reaction dynamics [15].

Today, CP-FTMW spectroscopy is frequently employed in combination with supersonic expansions, which significantly simplifies the recorded spectrum by reducing rotational temperature and narrowing the population distribution across the lowest rotational levels of the fundamental vibrational level [16–18]. Nonetheless, there are numerous examples where CP-FTMW spectroscopy has also been applied to record rotational spectra at room temperature using conventional cells [19–21]. This approach offers the advantage of studying the rotational spectra under conditions closer to the atmospheric environments, and enables the observation of rotational lines not present in molecular beam-based spectra and vibrationally excited states' rotational spectra. However, the spectra obtained at room temperature in conventional cells tend to be densely packed with rotational transitions, particularly for larger molecules with higher molecular masses. This density may complicate the spectral analysis, especially in the absence of reference data, making the assignment of transitions more challenging. In this work, we present a new investigation of the rotational spectrum of TFA at room temperature using a K-band chirped-pulse Fourier transform microwave (CP-FTMW) spectrometer in a conventional cell, operating in the 18–26 GHz frequency range. The newly acquired data, combined with those from previous investigations, are employed to perform a comprehensive global fit of the rotational spectrum of the molecule's vibrational ground state.

2. Experimental methods

TFA (CAS Registry Number 76-05-1; MW = 114.02 g/mol) was obtained from Merck with a declared purity 99% and used without further purification. TFA appears as a colourless liquid and its vapour pressure is 15.8 kPa at room conditions. The rotational spectrum was recorded using a commercial segmented K-Band chirped-pulse Fourier Transform Microwave spectrometer (CP-FTMW), also referenced as Fourier Transform Molecular Rotational Resonance spectrometer (FT-MRR) purchased from BrightSpec. The instrument works in the 18–26 GHz frequency region with an instantaneous bandwidth of 30 MHz and a repetition rate of 50 kHz using a 10 MHz rubidium frequency standard to maintain frequency stability. The recorded lines have an uncertainty of 30 kHz and transition lines separated by 300 kHz are distinguishable. To generate the chirped pulses, the system relies on a phase-locked loop synthesizer with arbitrary waveform generator (AWG) modulation, which is then amplified by a solid-state power amplifier (SSPA) delivering about 2 W. The spectrometer is coupled with a 65 cm long transmission cell with Teflon focusing lenses. The emitted signal, referred to as free induction decay (FID), is detected by a double-balanced heterodyne mixer connected to a 125 MS/s 14-bit Digitizer with FPGA Signal Averaging and real-time signal averaging capabilities. The sample is introduced into the spectrometer by collecting the headspace vapour from a vial, containing the sample, and fluxing it into the transmission cell using a system of rotary pump and diffusive pump. A constant flow from the vial to the cell was maintained by the pump system, ensuring a stable pressure of 2.5 mTorr and a temperature of 303 K. The spectrum has been recorded using a pulse of 0.4 μs with four hundred thousand signal averages.

3. Computational methods

Geometry optimization and vibrational frequency calculations on TFA were performed with the Gaussian16® software package (G16, Rev. A.03)[1] using the valence triple-zeta quality Dunning correlation

[1] Gaussian is a registered trademark of Gaussian, Inc. 340 Quinnipiac St. Bldg. 40 Wallingford, CT 06492 USA.

consistent polarized type basis set augmented with diffuse functions (aug-cc-pVTZ [22]) in combination with the Møller-Plesset second-order perturbation theory (MP2 [23]). The anharmonic force field was evaluated via the generalized second-order vibrational perturbation theory (GVPT2 [24,25]) and the corresponding output file can be found in the AMS Acta [26].

4. Results

The recorded spectrum of TFA, a prolate rotor ($\kappa = -0.53$), is reported in Fig. 1. Over 1000 transition lines with S/N ratio > 3 have been detected. Among them, 184 were assigned to the vibrational ground state, in particular 7 lines are μ_a-R-type and 4 are μ_b-R-type corresponding to lower $J = 2$–5, while 32 are μ_a-Q-type and 141 are μ_b-Q-type with lower $J = 8$–52. The list of the measured lines is reported in Table 1. The new set of lines has been used to perform a global fitting including all the previously measured rotational transition lines by direct diagonalization of Watson's asymmetrically reduced Hamiltonian in the I^r representation:

$$\hat{H} = \hat{H}_R + \hat{H}_{CD} \quad (1)$$

where $\hat{H}_R$ represents the rigid rotor and $\hat{H}_{CD}$ is the centrifugal distortion contribution. The fitting has been performed by means of the CALPGM program suite [27] using both S and A reductions to compare with results from previous works. According to the different experimental conditions, the following uncertainties were applied to the lines in the fit: 150 kHz for Stolwijk and van Eijck dataset [7], 3 kHz for both Antolinez et al. [8] and Ouyang et al. [9] datasets and 30 kHz for the lines recorded with the K-Band CP-FTMW spectrometer. Due to some overlap in the frequency ranges of the four datasets considered, certain transition lines were observed multiple times. As a result, and considering the consistent error estimation on recorded lines, the assignments from Antolinez et al. [8] and Ouyang et al. [9] were both incorporated into the fitting, with each common transition being weighted at 0.5. For lines common to both our study and van Ejick and Stolwijk work [7], we opted to consider only the frequencies recorded with our instrument due to its significantly lower measurement error. Table 2 reports the fitted spectroscopic parameters in the S-reduction compared with the fitted values reported by Ouyang et al. [9]. Table 3 lists the fitted spectroscopic parameters in the A-reduction compared to the results reported by Stolwijk and Van Eijck [7] and Antolinez et al. [8]. The σ values reported in both tables represent the root mean square (RMS) deviations relative to the global fit. The RMS deviations for each dataset computed with the new fitting parameters are as follows: 106 kHz for the Stolwijk and Van Eijck dataset [7] using Watson A-reduction, 5 kHz for the Antolinez et al. dataset [8] using Watson A-reduction, and 7 kHz for the Ouyang et al. dataset [9] using Watson S-reduction. For the transition lines recorded in this study, the RMS values are 49 kHz using Watson S-reduction and 44 kHz using Watson A-reduction. In both tables, the theoretical values at MP2/aug-cc-pVTZ level of calculation are also given for comparison. The spectrum simulated using the fitted spectroscopic parameters in the S-reduction and the theoretical electric dipole moment components ($\mu_a = 1.71$ D and $\mu_b = 1.32$ D), is compared to the experimental one in Fig. 1, while Fig. 2 shows the distribution plot of the lower state J and K_a values of the rotational transitions considered for the fitting. The input and output fitting files are freely available in the AMS Acta repository [26].

5. Discussion

The inclusion of the sextic centrifugal distortion constants in the global fitting can fit all the observed transition lines well, showing the important role of these parameters when studying the spectrum at room temperature, where transitions originating from energy levels with high rotational quantum numbers are observed. Performing the global fitting without any sextic centrifugal distortion constants leads to a much larger standard deviation: for Watson's S-reduction we get a value of 613 kHz, compared to 59 kHz (Table 2), while for Watson A-reduction we get a value of 193 kHz against 62 kHz (Table 3).

All the fitted parameters are in good agreement with the calculated ones. It is interesting to notice how the inclusion of the h_3 sextic centrifugal distortion constant using Watson's S-reduction is able to fit all the new transition lines found, while the inclusion of all the other constants leads to a higher standard deviation. In the case of Watson's A-reduction three sextic constants (Φ_{JK}, Φ_{KJ} and ϕ_K) must be taken into account to get a comparable result.

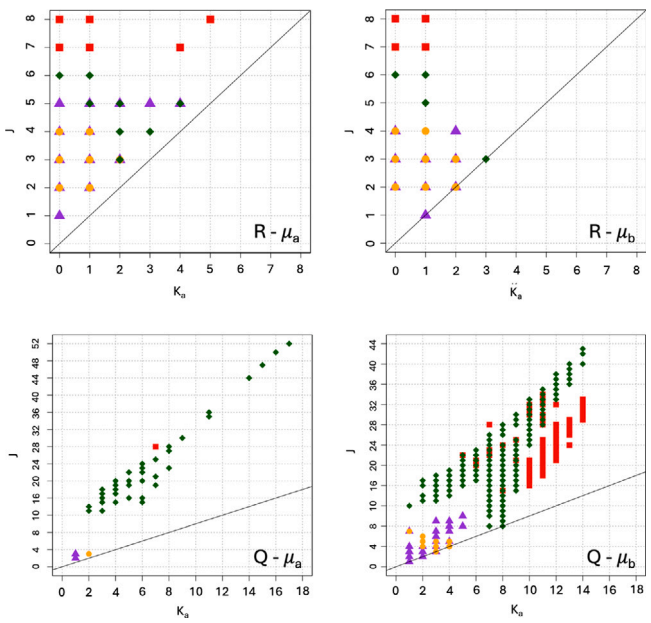

Fig. 2. Distribution plot of the fitted transition lines of TFA. Red squares refer to Stolwijk and van Eijck [7], purple triangles refer to Antolinez et al. [8], yellow circles refer to Ouyang et al. [9] and green rhombi refer to this work.

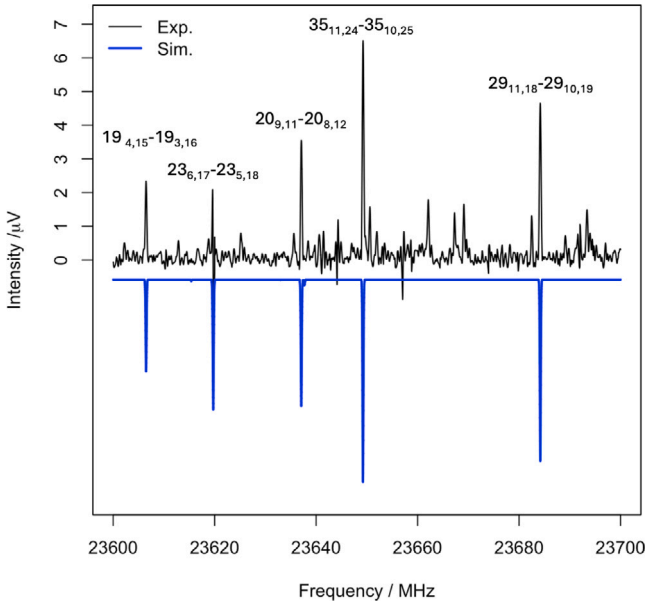

Fig. 3. Portion of the room temperature CP-FTMW spectrum of TFA recorded with 400,000 signal averages (black upper trace) with simulation at $T = 303$ K (blue lower trace).

Table 1
Measured frequencies (ν/MHz) and fitted deviations ($c - o$/MHz) of TFA.

$J''(K_a'', K_c'') - J'(K_a', K_c')$	ν	$c-o$	$J''(K_a'', K_c'') - J'(K_a', K_c')$	ν	$c-o$	$J''(K_a'', K_c'') - J'(K_a', K_c')$	ν	$c-o$
14(4,11)–14(3,12)	18 001.62	0.03	35(12,23)–35(11,24)	21 294.80	0.01	19(4,15)–19(3,16)	23 606.48	0.00
29(10,19)–29(9,20)	18 013.70	0.02	34(11,23)–34(10,24)	21 316.57	0.04	23(6,17)–23(5,18)	23 619.61	−0.11
28(9,19)–28(8,20)	18 270.26	0.02	20(5,15)–20(5,16)	21 317.46	−0.02	20(9,11)–20(8,12)	23 637.09	0.02
21(6,15)–21(5,16)	18 270.66	−0.12	20(7,14)–20(6,15)	21 350.49	0.03	35(11,24)–35(10,25)	23 649.25	0.02
30(10,20)–30(9,21)	18 397.19	0.13	16(4,13)–16(3,14)	21 398.45	0.02	29(11,18)–29(10,19)	23 684.18	−0.01
4(3,1)–3(3,0)	18 499.33	0.06	19(6,14)–19(5,15)	21 474.60	0.01	33(12,21)–33(11,22)	23 739.77	−0.01
13(2,11)–13(2,12)	18 552.03	−0.02	18(4,14)–18(4,15)	21 479.37	0.02	23(8,16)–23(7,17)	23 754.37	0.03
13(2,11)–13(1,12)	18 560.84	0.02	36(12,24)–36(11,25)	21 495.54	0.04	5(2,3)–4(2,2)	23 824.84	0.01
28(10,18)–28(9,19)	18 589.22	0.02	20(5,15)–20(4,16)	21 522.27	0.02	21(5,16)–21(4,17)	23 841.68	0.00
14(7,7)–14(6,8)	18 627.11	0.02	18(4,14)–18(3,15)	21 547.15	0.01	28(8,20)–28(8,21)	23 875.87	0.02
13(3,11)–13(2,12)	18 734.32	0.03	3(3,1)–2(2,0)	21 576.69	0.00	22(7,16)–22(6,17)	23 896.05	0.09
13(3,11)–13(1,12)	18 743.13	0.06	26(10,16)–26(9,17)	21 615.48	0.04	37(13,24)–37(12,25)	23 897.01	−0.06
17(6,12)–17(5,13)	18 893.48	0.18	30(9,21)–30(9,22)	21 625.51	0.03	16(2,14)–16(1,15)	23 972.12	−0.02
19(8,11)–19(7,12)	18 908.08	0.06	27(8,19)–27(7,20)	21 746.42	0.02	19(5,15)–19(4,16)	23 974.79	−0.01
4(2,2)–3(2,1)	18 924.50	0.01	30(11,19)–30(10,20)	21 823.77	−0.01	16(3,14)–16(2,15)	23 989.92	−0.02
26(8,18)–26(7,19)	18 969.25	0.03	19(8,12)–19(7,13)	21 832.81	0.02	19(5,15)–19(3,16)	24 006.68	0.00
16(5,12)–16(4,13)	18 991.14	0.00	18(8,11)–18(7,12)	21 887.69	0.02	36(11,25)–36(11,26)	24 239.53	−0.06
19(5,14)–19(4,15)	19 030.58	0.01	5(1,5)–4(0,4)	21 902.90	−0.05	40(13,27)–40(12,28)	24 317.89	0.01
15(3,12)–15(3,13)	19 123.03	0.00	20(8,13)–20(7,14)	21 947.22	0.06	22(9,14)–22(8,15)	24 347.85	0.01
15(3,12)–15(2,13)	19 163.65	−0.02	17(8,10)–17(7,11)	22 052.79	−0.07	23(9,15)–23(8,16)	24 416.80	0.02
17(4,13)–17(4,14)	19 207.08	0.11	32(10,22)–32(9,23)	22 112.64	0.03	19(9,10)–19(8,11)	24 426.09	0.04
13(7,6)–13(6,7)	19 210.87	−0.12	34(12,22)–34(11,23)	22 130.17	0.00	21(9,13)–21(8,14)	24 450.28	0.04
16(7,10)–16(6,11)	19 267.49	0.01	25(7,18)–25(7,19)	22 200.11	0.00	50(16,34)–50(16,35)	24 515.21	−0.07
15(7,9)–15(6,10)	19 272.92	0.00	15(3,13)–15(2,14)	22 232.10	0.04	42(14,28)–42(13,29)	24 576.93	−0.03
16(5,12)–16(3,13)	19 273.83	−0.04	18(5,14)–18(4,15)	22 232.53	0.01	20(9,12)–20(8,13)	24 664.47	0.03
17(4,13)–17(3,14)	19 347.54	0.01	15(3,13)–15(1,14)	22 233.53	−0.10	24(9,16)–24(8,17)	24 711.62	0.02
17(7,11)–17(6,12)	19 429.23	0.04	16(8,9)–16(7,10)	22 273.92	−0.02	21(6,16)–21(5,17)	24 721.63	−0.03
23(9,14)–23(8,15)	19 536.10	0.08	21(8,14)–21(7,15)	22 284.17	0.03	28(8,20)–28(7,21)	24 723.71	0.01
12(7,5)–12(6,6)	19 597.64	0.00	15(8,7)–15(7,8)	22 321.42	0.01	18(3,15)–18(3,16)	24 863.54	0.08
52(17,35)–52(17,36)	19 643.54	0.15	15(8,8)–15(7,9)	22 508.40	0.01	18(3,15)–18(2,16)	24 867.06	0.01
32(11,21)–32(10,22)	19 655.85	0.00	21(7,15)–21(6,16)	22 511.20	0.03	24(10,14)–24(9,15)	24 891.30	0.06
15(4,12)–15(3,13)	19 670.50	0.02	21(9,12)–21(8,13)	22 550.09	0.03	24(8,17)–24(7,18)	24 893.25	0.07
35(11,24)–35(11,25)	19 694.42	0.04	44(14,30)–44(14,31)	22 641.17	−0.09	18(4,15)–18(3,16)	24 931.25	0.00
15(4,12)–15(2,13)	19 711.17	0.05	14(8,6)–14(7,7)	22 654.45	0.00	19(9,11)–19(8,12)	24 935.80	0.08
12(7,6)–12(6,7)	19 737.27	−0.07	14(8,7)–14(7,8)	22 728.37	0.02	33(10,23)–33(9,24)	25 057.16	−0.03
31(10,21)–31(9,22)	19 800.93	0.04	37(12,25)–37(11,26)	22 821.07	−0.01	38(12,26)–38(11,27)	25 169.26	−0.02
18(7,12)–18(6,13)	19 810.23	0.06	22(8,15)–22(7,16)	22 881.52	0.04	18(9,10)–18(8,11)	25 221.12	0.01
11(7,4)–11(6,5)	19 854.38	−0.03	25(7,18)–25(6,19)	22 883.41	−0.02	25(9,17)–25(8,18)	25 271.87	0.00
27(10,17)–27(9,18)	19 902.73	−0.06	13(8,5)–13(7,6)	22 893.02	0.01	17(9,8)–17(8,9)	25 393.56	0.01
11(7,5)–11(6,6)	19 904.44	0.01	13(8,6)–13(7,7)	22 919.28	−0.04	23(7,17)–23(6,18)	25 459.26	0.07
33(11,22)–33(10,23)	19 949.48	0.04	38(13,25)–38(12,26)	22 931.67	0.00	20(4,16)–20(4,17)	25 549.13	0.01
10(7,3)–10(6,4)	20 028.56	−0.01	17(3,14)–17(2,15)	23 025.56	0.00	28(11,17)–28(10,18)	25 568.19	0.03
24(7,17)–24(6,18)	20 033.29	0.05	39(13,26)–39(12,27)	23 037.44	0.00	6(0,6)–5(1,5)	25 645.21	0.09
10(7,4)–10(6,5)	20 044.07	−0.04	20(6,15)–20(5,16)	23 038.75	−0.01	36(13,23)–36(12,24)	25 650.98	−0.08
18(6,13)–18(5,14)	20 077.54	0.02	5(4,2)–4(4,1)	23 055.98	−0.01	26(7,19)–26(6,20)	25 652.01	0.00
18(8,10)–18(7,11)	20 180.67	0.00	12(8,4)–12(7,5)	23 068.24	0.01	40(14,26)–40(13,27)	25 661.60	−0.10
16(6,11)–16(4,12)	20 234.51	0.00	12(8,5)–12(7,6)	23 076.58	0.03	16(9,7)–16(8,8)	25 694.62	0.01
27(8,19)–27(8,20)	20 243.85	0.09	17(4,14)–17(3,15)	23 157.91	−0.01	6(1,6)–5(1,5)	25 730.45	0.01
31(11,20)–31(10,21)	20 361.03	0.00	11(8,3)–11(7,4)	23 198.73	−0.08	16(9,8)–16(8,9)	25 732.83	−0.02
14(2,12)–14(2,13)	20 390.18	0.05	11(8,4)–11(7,5)	23 201.11	0.02	17(2,15)–17(1,16)	25 739.11	−0.10
14(2,12)–14(1,13)	20 393.86	0.00	20(6,15)–20(4,16)	23 243.52	−0.01	17(3,15)–17(1,16)	25 747.28	−0.14
19(7,13)–19(6,14)	20 446.43	0.16	10(8,2)–10(7,3)	23 296.23	0.02	20(5,16)–20(4,17)	25 753.96	0.07
22(6,16)–22(6,17)	20 455.21	0.03	10(8,3)–10(7,4)	23 296.67	−0.07	43(14,29)–43(13,30)	25 809.68	−0.10
14(3,12)–14(2,13)	20 477.51	0.01	23(6,17)–23(6,18)	23 339.94	−0.03	6(0,6)–5(0,5)	25 828.96	0.03
29(9,20)–29(8,21)	20 554.52	0.03	25(10,15)–25(9,16)	23 366.27	0.06	6(1,6)–5(0,5)	25 914.24	−0.01
17(5,13)–17(4,14)	20 557.69	−0.05	9(8,1)–9(7,2)	23 368.03	0.00	24(6,18)–24(6,19)	25 919.51	−0.01
15(6,10)–15(4,11)	20 851.35	0.04	9(8,2)–9(7,3)	23 368.03	−0.10	15(9,6)–15(8,7)	25 924.29	0.01
22(6,16)–22(5,17)	20 989.11	0.01	30(9,21)–30(8,22)	23 418.68	0.02	15(9,7)–15(8,8)	25 937.81	−0.03
16(3,13)–16(3,14)	21 115.70	0.00	8(8,0)–8(7,1)	23 419.76	−0.05	22(5,17)–22(5,18)	25 946.20	−0.05
16(3,13)–16(2,14)	21 134.14	0.00	8(8,1)–8(7,2)	23 419.76	−0.07	22(5,17)–22(4,18)	25 995.46	0.00
22(9,13)–22(8,14)	21 147.22	0.01	5(1,4)–4(1,3)	23 447.18	−0.02			
17(8,9)–17(7,10)	21 153.94	0.03	47(15,32)–47(15,33)	23 582.99	−0.10			

Fig. 3 presents a segment of the observed spectrum alongside the predicted spectrum calculated using the fitted parameters in Watson's *S*-reduction at a temperature of T = 303 K. Overall, there is good agreement between the experimental and predicted relative intensities of the transition lines. The only notable discrepancy is observed in the $23_{6,17} - 23_{5,18}$ transition, where the experimental intensity appears lower than predicted. However, this variation can be attributed to the experimental peak being distorted by a signal spike caused by instrumental fluctuations.

The transitions measured in this study could be predicted with significantly lower accuracy using the previously available spectroscopic constants, leading to errors up to 5 MHz. An example of this is reported in Fig. 4, where two portions of the experimental spectrum of TFA are compared with the prediction calculated using both our and Stolwijk et al. [7] Watson's *A* fits.

6. Conclusions

The rotational spectrum of TFA at room temperature has been measured by means of the K-Band CP-FTMW spectrometer and the transition lines of the species have been assigned. The spectrum has

Table 2
Experimental and theoretical rotational spectroscopy parameters of TFA in the *S*-reduction and I^r representation.

Parameter[a]	Literature[b]	This work	Calc.[c]
A/MHz	3865.13430(89)[d]	3865.1317(2)	3849.3811
B/MHz	2498.79448(56)	2498.7939(2)	2505.9531
C/MHz	2075.20197(63)	2075.2010(2)	2073.9498
D_J/kHz	0.966(22)	0.988(5)	0.9830
D_{JK}/kHz	−0.938(62)	−0.975(1)	−1.0733
D_K/kHz	0.466(61)	0.451(4)	0.5146
d_1/kHz	−0.0483(69)	−0.0519(1)	−0.0493
d_2/kHz	0.3471(51)	0.34792(5)	0.3652
H_J/mHz	(–)	(–)	−0.9239
H_{JK}/mHz	(–)	(–)	−23.5007
H_{KJ}/mHz	(–)	(–)	50.8721
H_K/mHz	(–)	(–)	−26.3819
h_1/mHz	(–)	(–)	−2.1947
h_2/mHz	(–)	(–)	0.4790
h_3/mHz	(–)	1.99(6)	2.2093
N	33	347	(–)
σ/kHz	1.5	59	(–)

[a] A, B, and C are the rotational constants. D_J, D_{JK}, D_K, d_1 and d_2 are the quartic centrifugal distortion constants. H_J, H_{JK}, H_{JK}, H_K, h_1, h_2 and h_3 are the sextic centrifugal distortion constants. N is the number of transition lines fitted. σ is the standard deviation of the fit.
[b] From Ouyang et al. [9].
[c] MP2/aug-cc-pVTZ.
[d] Error in the unit of the last digit.

Table 3
Experimental and theoretical rotational spectroscopy parameters of TFA in the *A*-reduction and I^r representation.

Parameter[a]	Literature[b]	Literature[c]	This work	Calc.[d]
A/MHz	3865.098(5)[e]	3865.13293(11)	3865.1352(2)	3849.3811
B/MHz	2498.738(4)	2498.76962(8)	2498.7716(2)	2505.9531
C/MHz	2075.188(3)	2075.21871(7)	2075.2205(2)	2073.9498
Δ_J/kHz	(–)	0.2617(18)	0.292(5)	0.2523
Δ_{JK}/kHz	3.20(1)	3.1856(25)	3.201(2)	3.3105
Δ_K/kHz	−2.97(2)	−2.9924(71)	−3.030(5)	−3.1386
δ_J/kHz	0.055(2)	0.05108(27)	0.0511(1)	0.0493
δ_k/kHz	−10.47(2)	−10.3632(39)	−10.369(2)	−10.5498
Φ_J/mHz	(–)	(–)	(–)	0.0342
Φ_{JK}/Hz	(–)	(–)	0.217(2)	0.2260
Φ_{KJ}/Hz	(–)	(–)	−0.568(9)	−0.7950
Φ_K/Hz	(–)	(–)	(–)	0.5691
ϕ_J/mHz	(–)	(–)	(–)	0.0146
ϕ_{JK}/mHz	(–)	(–)	(–)	−6.0657
ϕ_K/Hz	(–)	(–)	0.79(1)	0.7457
N	99	50	347	(–)
σ/kHz	160	36	62	(–)

[a] A, B, and C are the rotational constants. Δ_J, Δ_{JK}, Δ_K, δ_J and δ_K are the quartic centrifugal distortion constants. Φ_J, Φ_{JK}, Φ_{JK}, Φ_K, ϕ_J, ϕ_{JK} and ϕ_K are the sextic centrifugal distortion constants. N is the number of transition lines fitted. σ is the standard deviation of the fit.
[b] From Stolwijk and van Eijck [7].
[c] From Antolinez et al. [8].
[d] MP2/aug-cc-pVTZ.
[e] Error in the unit of the last digit.

been recorded using similar conditions to the ones used by Stolwijk et al. [7], overlapping with the same spectral range studied. However, because of the different instrumentation used, our measurements revealed a significantly larger number of rotational transitions that Stolwijk's study did not report. Analysing this type of spectrum is particularly challenging due to the high density of Q-type rotational transitions involving rotational states with large J quantum numbers. This is especially true for heavy molecules like TFA, where the contribution from low-lying vibrational states plays a significant role, further complicating the interpretation of the spectrum. However, by leveraging the extensive dataset of transition lines from previous studies for the vibrational ground state, we were able to generate more accurate predictions of the rotational spectrum, allowing us to assign the newly

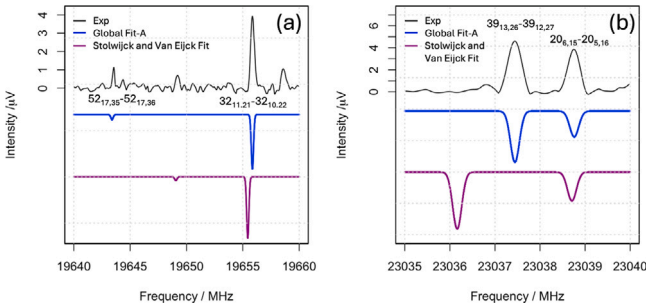

Fig. 4. Portions of the room temperature CP-FTMW spectrum of TFA recorded with 400,000 signal averages (black upper trace) with simulations at T = 303 K using global fit-A model (blue middle trace) and using Stolwijk et al. [7] (purple lower trace).

observed transition lines. In particular, several high-J Q-type transition lines have been assigned that showed displacements up to 5 MHz with respect to previous predictions. These newly measured lines will improve line catalogues for atmospheric monitoring.

CRediT authorship contribution statement

Greta Naso: Investigation. **Filippo Baroncelli:** Writing – review & editing, Writing – original draft, Visualization, Supervision, Investigation, Formal analysis, Data curation, Conceptualization. **Luca Evangelisti:** Writing – review & editing, Validation. **Assimo Maris:** Writing – original draft, Supervision, Formal analysis, Data curation, Conceptualization. **Sonia Melandri:** Writing – review & editing, Supervision, Project administration, Methodology, Funding acquisition, Conceptualization.

Declaration of competing interest

The authors declare that they have no known competing financial interests or personal relationships that could have appeared to influence the work reported in this paper.

Acknowledgements

We acknowledge funding from MUR, Italy through grant EUROSTARS 3 CoD01 2021 (CUP: J53C22001060001) for the CLEANDROP project and the CINECA award under the ISCRA initiative, for the availability of high-performance computing resources and support. We thank the University of Bologna, Italy for financial support (RFO, Ricerca Fondamentale Orientata).

Data availability

The data are available at https://doi.org/10.6092/unibo/amsacta/8016.

References

[1] H.P.H. Arp, A. Gredelj, J. Glüge, M. Scheringer, I.T. Cousins, The global threat from the irreversible accumulation of trifluoroacetic acid (TFA), Environ. Sci. Technol. 58 (45) (2024) 19925–19935, http://dx.doi.org/10.1021/acs.est.4c06189.
[2] F. Freeling, M.K. Björnsdotter, Assessing the environmental occurrence of the anthropogenic contaminant trifluoroacetic acid (TFA), Curr. Opin. Green Sustain. Chem. J. 41 (2023) 100807, http://dx.doi.org/10.1016/j.cogsc.2023.100807.
[3] K.R. Solomon, G.J.M. Velders, S.R. Wilson, S. Madronich, J. Longstreth, P.J. Aucamp, J.F. Bornman, Sources, fates, toxicity, and risks of trifluoroacetic acid and its salts: Relevance to substances regulated under the montreal and kyoto protocols, J. Toxicol. Env. Heal. B 19 (7) (2016) 289–304, http://dx.doi.org/10.1080/10937404.2016.1175981.

[4] N.R. Walker, New opportunities and emerging themes of research in microwave spectroscopy, Philos. Trans. R Soc. A 365 (1861) (2007) 2813–2828, http://dx.doi.org/10.1098/rsta.2007.0001.
[5] C. Gibbins, A. Dawkins, B. Maddison, Microwave remote-sensing measurements of upper-atmospheric water vapour and ozone from a balloon-borne platform, Planet. Space Sci. 36 (6) (1988).
[6] B.J. Drouin, D.J. Nemchick, A. Nole, A. Tang, C.-T.M. Wu, N. Khiabani, M. Alonso, M.-C.F. Chang, Dual-band Fourier-transform millimeter-wave spectrometry for in situ gas sensing, Planet. Sci. J. 4 (6) (2023) 100, http://dx.doi.org/10.3847/PSJ/acd348.
[7] V. Stolwijk, B. van Eijck, Microwave spectra and barriers to internal rotation of trifluoroacetic acid and trifluoroacetyl fluoride, J. Mol. Spectrosc. 113 (1) (1985) 196–207, http://dx.doi.org/10.1016/0022-2852(85)90130-4.
[8] S. Antolinez, J.L. Alonso, H. Dreizler, D.H. Sutter, Trifluoroacetic acid; r_0-structure, partial substitution structure and deuterium nuclear quadrupole coupling studied by molecular beam microwave Fourier transform spectroscopy and by ab initio calculations, Z. Nat.forsch. A 54 (8–9) (1999) 524–538, http://dx.doi.org/10.1515/zna-1999-8-915.
[9] B. Ouyang, T.G. Starkey, B.J. Howard, High-resolution microwave studies of ring-structured complexes between trifluoroacetic acid and water, J. Phys. Chem. A 111 (28) (2007) 6165–6175, http://dx.doi.org/10.1021/jp071130y.
[10] G. Grubbs, A. Serrato, D.A. Obenchain, S. Cooke, S.E. Novick, W. Lin, The rotational spectrum of perfluoropropionic acid, J. Mol. Spectrosc. 275 (2012) 1–4, http://dx.doi.org/10.1016/j.jms.2012.04.003.
[11] J. Thomas, A. Serrato III, W. Lin, W. Jäger, Y. Xu, Perfluorobutyric acid and its monohydrate: A chirped pulse and cavity based Fourier transform microwave spectroscopic study, Chem. Eur. J. 20 (20) (2014) 6148–6153, http://dx.doi.org/10.1002/chem.201304321.
[12] A.M. Pejlovas, K. Li, S.G. Kukolich, W. Lin, Microwave spectrum of perfluoropentanoic acid, Chem. Phys. Lett. 610–611 (2014) 82–85, http://dx.doi.org/10.1016/j.cplett.2014.06.053.
[13] R.N. Schilberg, S. Wei, S. Twagirayezu, J.L. Neill, Conformational dynamics of perfluorooctanoic acid (PFOA) studied by molecular rotational resonance (MRR) spectroscopy, Chem. Phys. Lett. 778 (2021) 138789, http://dx.doi.org/10.1016/j.cplett.2021.138789.
[14] G.G. Brown, B.C. Dian, K.O. Douglass, S.M. Geyer, B.H. Pate, The rotational spectrum of epifluorohydrin measured by chirped-pulse Fourier transform microwave spectroscopy, J. Mol. Spectrosc. 238 (2) (2006) 200–212, http://dx.doi.org/10.1016/j.jms.2006.05.003.
[15] G.B. Park, R.W. Field, Perspective: The first ten years of broadband chirped pulse Fourier transform microwave spectroscopy, J. Chem. Phys. 144 (20) (2016) 200901, http://dx.doi.org/10.1063/1.4952762.
[16] S. Blanco, J.C. López, A. Maris, Terpenoids: shape and non-covalent interactions. The rotational spectrum of cis-verbenol and its 1:1 water complex, Phys. Chem. Chem. Phys. 22 (2020) 5729–5734, http://dx.doi.org/10.1039/D0CP00086H.
[17] D. Lv, W. Li, L. Evangelisti, I. Usabiaga, C. Calabrese, A. Maris, S. Melandri, G. Wang, M. Zhou, Rotational spectroscopy probes lone pair$\cdots\pi$-hole interactions in hexafluorobenzene-tertiary alkylamines complexes, J. Phys. Chem. Lett. 14 (23) (2023) 5335–5342, http://dx.doi.org/10.1021/acs.jpclett.3c00882.
[18] C. Calabrese, A. Maris, I. Uriarte, E.J. Cocinero, S. Melandri, Effects of chlorination on the tautomeric equilibrium of 2-hydroxypyridine: Experiment and theory, Chem. Eur. J. 23 (15) (2017) 3595–3604, http://dx.doi.org/10.1002/chem.201604891.
[19] B. Reinhold, I. Finneran, S. Shipman, Room temperature chirped-pulse Fourier transform microwave spectroscopy of anisole, J. Mol. Spectrosc. 270 (2) (2011) 89–97, http://dx.doi.org/10.1016/j.jms.2011.10.002.
[20] C.A. Dim, C. Sorrells, A.O. Hernandez-Castillo, K.N. Crabtree, K_a-band rotational spectroscopy of succinimide and N-chlorosuccinimide, J. Phys. Chem. A 128 (45) (2024) 9754–9762, http://dx.doi.org/10.1021/acs.jpca.4c06004.
[21] K.N. Crabtree, J.H. Westerfield, C.A. Dim, K.S. Meyer, S.L. Johansen, Z.S. Buchanan, P.A. Stucky, Rotational spectroscopy of methyl tert-butyl ether with a new K_a band chirped-pulse Fourier transform microwave spectrometer, Phys. Chem. Chem. Phys. 26 (2024) 13694–13709, http://dx.doi.org/10.1039/D4CP00797B.
[22] T.H. Dunning Jr., Gaussian basis sets for use in correlated molecular calculations. I. The atoms boron through neon and hydrogen, J. Chem. Phys. 90 (2) (1989) 1007–1023, http://dx.doi.org/10.1063/1.456153.
[23] C. Møller, M.S. Plesset, Note on an approximation treatment for many-electron systems, Phys. Rev. 46 (7) (1934) 618–622, http://dx.doi.org/10.1103/PhysRev.46.618.
[24] V. Barone, Anharmonic vibrational properties by a fully automated second-order perturbative approach, J. Chem. Phys. 122 (1) (2005) 014108, http://dx.doi.org/10.1063/1.1824881.
[25] J. Bloino, V. Barone, A second-order perturbation theory route to vibrational averages and transition properties of molecules: general formulation and application to infrared and vibrational circular dichroism spectroscopic, J. Chem. Phys. 136 (2012) 124108, http://dx.doi.org/10.1063/1.3695210.
[26] G. Naso, F. Baroncelli, S. Melandri, L. Evangelisti, A. Maris, Reference data for isolated trifluoroacetic acid, Univ. Bologna (2024) http://dx.doi.org/10.6092/unibo/amsacta/8016.
[27] H.M. Pickett, The fitting and prediction of vibration-rotation spectra with spin interactions, J. Mol. Spectrosc. 148 (2) (1991) 371–377, http://dx.doi.org/10.1016/0022-2852(91)90393-O.